PERSPECTIVE | JANUARY 09 2026

Momentum microscopy and its applications

Ying-Jiun Chen ; Carsten Wiemann ; Wei-Sheng Chiu ; Christoph Schlueter ; Claus M. Schneider ; Christian Tusche

Appl. Phys. Lett. 128, 010503 (2026)
https://doi.org/10.1063/5.0304110

Applied Physics Letters PERSPECTIVE pubs.aip.org/aip/apl

Momentum microscopy and its applications

Cite as: Appl. Phys. Lett. **128**, 010503 (2026); doi: 10.1063/5.0304110
Submitted: 26 September 2025 · Accepted: 22 December 2025 ·
Published Online: 9 January 2026

Ying-Jiun Chen,[1,2,a] Carsten Wiemann,[1] Wei-Sheng Chiu,[1,3] Christoph Schlueter,[4] Claus M. Schneider,[1,3] and Christian Tusche[1,3,b]

AFFILIATIONS

[1]Peter Grünberg Institut (PGI-6), Forschungszentrum Jülich, 52425 Jülich, Germany
[2]Ernst Ruska-Centre for Microscopy and Spectroscopy with Electrons (ERC-1), Forschungszentrum Jülich, 52425 Jülich, Germany
[3]Fakultät für Physik, Universität Duisburg-Essen, 47057 Duisburg, Germany
[4]Deutsches Elektronen-Synchrotron DESY, Notkestr. 85, 22607 Hamburg, Germany

[a]Electronic mail: yi.chen@fz-juelich.de
[b]Author to whom correspondence should be addressed: c.tusche@fz-juelich.de

ABSTRACT

Experimental tools lie at the heart of discovering science. The ability to develop transformative tools that enable unprecedented insight into the physical and chemical properties of materials will significantly advance many fields of scientific research. The visionary aim of probing and visualizing the quantum degree of freedom of materials requires a comprehensive access to orbital symmetries, spin, and dynamics of quantum states across large regions of the momentum space. Momentum microscopy stands as the most advanced experimental technique for probing the electronic structure of materials, uniquely unifying spin, orbital, time, spatial, momentum, and energy information in a single experiment. In this Perspective, we provide an overview of momentum microscopy and its applications. We review state-of-the-art all-in-one photoemission experiments and highlight recent advances enabled by momentum microscopy. We conclude this Perspective with the exciting future directions currently developing in the field.

I. INTRODUCTION

Grand scientific challenges drive the creation of advanced tools, and conversely, the advent of advanced tools facilitates the exploration of previously inconceivable frontiers in science. In the quest for smaller, faster, and more energy efficient information technology, advanced materials with innovative functionalities are needed. Exploiting unconventional quantum states is nowadays a widely anticipated pathway to revolutionary advances in quantum computing and low-power devices.

However, experimentally probing the key physical and chemical properties of advanced materials across multiple dimensions still remains a significant challenge. In this context, momentum microscopy has emerged as a transformative tool for visualizing quantum states and understanding their collective behavior, bringing together spatial, momentum, energy, spin, orbital, and temporal information—all captured within a single, unified experiment, as illustrated in Fig. 1.[1–6] This *Perspective* highlights recent advances in momentum microscopy and its growing impact in the field of quantum materials, ushering in a bright era in quantum metrology for next-generation functional materials.

II. ADVANCES IN MOMENTUM MICROSCOPY

Recent advances in momentum microscopy have established it as a groundbreaking methodology that merges the capabilities of photoemission spectroscopy and electron microscopy into a single instrument. This combination enables a simultaneous acquisition of both electronic and spatial information.[1,3,7,14,15] Unlike conventional angle-resolved photoemission spectroscopy (ARPES), momentum microscopy directly maps the momentum of emitted photoelectrons without the need to mechanically scan larger regions of momentum space or to probe along different high-symmetry axes of the Brillouin zone (BZ). Instead, an advanced cathode lens captures two-dimensional (k_x, k_y),[1,16,17] or three-dimensional (k_x, k_y, E_B)[17–21] maps of the photoelectron spectral function, simultaneously. These maps represent slices through the valence electronic states across the full surface Brillouin zone (SBZ), providing comprehensive and intuitive access to a material's electronic properties.

Momentum microscopy leverages the imaging properties of an electron microscope. Without the need for focused photon beams, it inherently provides spatially resolved electron micrographs, alongside momentum-resolved images from confined surface areas.[3,14,15]

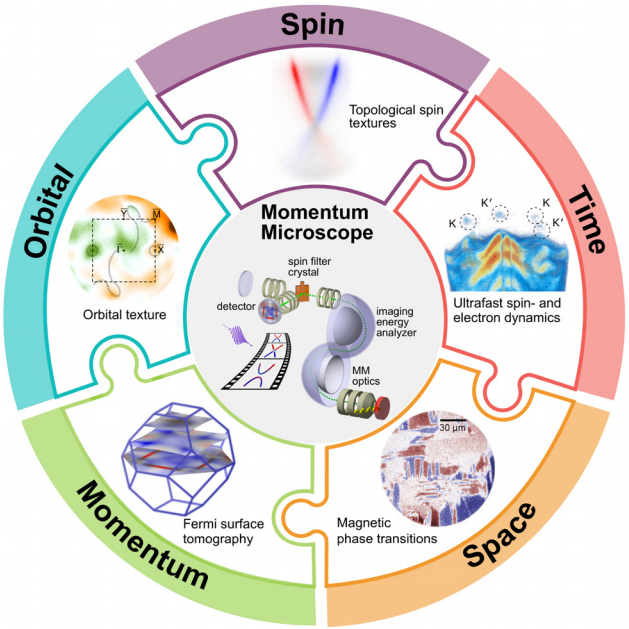

FIG. 1. The all-in-one photoemission experiment combines information on space,[7] momentum,[8] spin,[9] time,[10,11] and orbital[12] in the femtosecond regime.[10,11] The momentum microscope[1,2] bridges all these dimensions in a single experiment.

This enables us to study variations in the electronic structure across inhomogeneous samples, including domain-specific band dispersions and buried interfaces in complex heterostructures.[3,14,15,22–24] As a result, it allows for correlative investigations of electronic properties with nanometer spatial resolution, including techniques such as dark field imaging[15] that were previously inaccessible.

III. APPLICATIONS

The need for multidimensional characterization has driven several fundamental advances in electron optical design, energy analyzers, and imaging spin detectors.[1,4–6,16,17] These elements—shown at the center of Fig. 1—are central to what makes momentum microscopy an exceptionally powerful tool for addressing the microscopy and spectroscopy needs of emerging functional materials. In the following, we highlight key results that demonstrate the distinctive capabilities of this technique.

A. Zoomable momentum-space images

In a momentum microscope, a linearly scaled momentum image of the photoelectron distribution is already formed by the objective lens that immerses the sample in an accelerating electric field. As shown in Fig. 2(b), electrons that are emitted into the complete solid angle (2π sr) above the surface are collected under a finite angle θ'. Unlike conventional electron spectroscopy methods, this allows us to measure emission angles up to $\pm 90°$ with the maximum momentum $k_{||}$ that can be found at a given kinetic energy.[1,17] In particular, the direct momentum space imaging allows us to precisely select the field-of-view—for both real and momentum space.[1,17]

Figure 2(c) shows momentum microscopy measurements at the Fermi energy of a clean Au(111) surface at different momentum space magnifications. The first image was acquired using He-II radiation with a photon energy of $h\upsilon = 40.8$ eV, while the image captures the entire momentum disk with a total diameter of ≈ 6 Å^{-1}. The middle and right images show a magnification of the first SBZ and the detail of the Shockley surface state of Au(111), respectively. Both measurements were acquired using He-I radiation with a photon energy of $h\upsilon = 21.2$ eV. The surface state exhibits the characteristic Rashba-type splitting into two spin subbands.[1,25,26] The splitting manifests itself as two concentric circular bands in the Fermi surface contour and is already evident in the full image of the SBZ. A quantitative measurement of the spectral linewidth is readily obtained from the magnified details in the right panel of Fig. 2(c).[1]

B. Spin states in advanced materials

Comprehensive access to spin-resolved band structures became feasible by imaging spin filters:[13,27–30] The reflection of low-energy electrons at a spin-polarizing single-crystal surface, outlined in Fig. 3(a), allows one to measure 1000 s of spin-resolved data points simultaneously.[1,27] Instead of detecting a single data point, this concept allows the parallel imaging of spin-resolved two-dimensional electron distributions. Imaging spin filters have boosted the efficiency of electron spin detection by more than 5 orders of magnitude compared to the traditional Mott spin detector.[13,17,31] The spin-resolved spectral function in the momentum space and spin-filtered real-space PEEM (Photoelectron Emission Microscopy) images are now becoming routinely accessible. In the following, we highlight representative examples of their use in addressing spin-dependent phenomena across various classes of materials.

1. Imaging magnetic phase transitions

Spin-resolved PEEM imaging enables the real-time observation of magnetic domains, giving access to anisotropies and phase transitions.[7] A representative example is the prototypical ferromagnet magnetite (Fe_3O_4), characteristic for its simultaneous change in crystal structure, as well as electric and magnetic properties through the Verwey transition.[33] Spin-resolved PEEM images reveal the effect of the phase transition in the magnetic structure: while domain walls in the metallic high-temperature phase [Fig. 3(b)] align along the compact ⟨110⟩ directions, domains become elongated along the y axis in the insulating low-temperature phase [Fig. 3(c)].[7] Sharpened domain boundaries further support an increase in magnetocrystalline anisotropy in the monoclinic low-temperature phase.[34]

The use of an imaging spin filter allows one to measure spin-resolved spatial images with a resolution close to that of regular PEEM images on the order of a few tens of nanometers.[1,35,36] However, the actual resolution can vary depending on the sample under investigation. The high energy resolution of the momentum microscope provides additional information, such as probing spin polarization at specific electronic states. Momentum microscopy further allows us to extend the study to accompanying changes of the electronic bands or the Fermi surface. Such combined studies are expected to provide fresh insight into the mechanisms that lead to metal–insulator transition as well as magnetic phase transitions.

2. Ultrathin hybrid ferromagnets

Spin-resolving momentum microscopy has proven to be a valuable tool for identifying spin-dependent interaction channels and

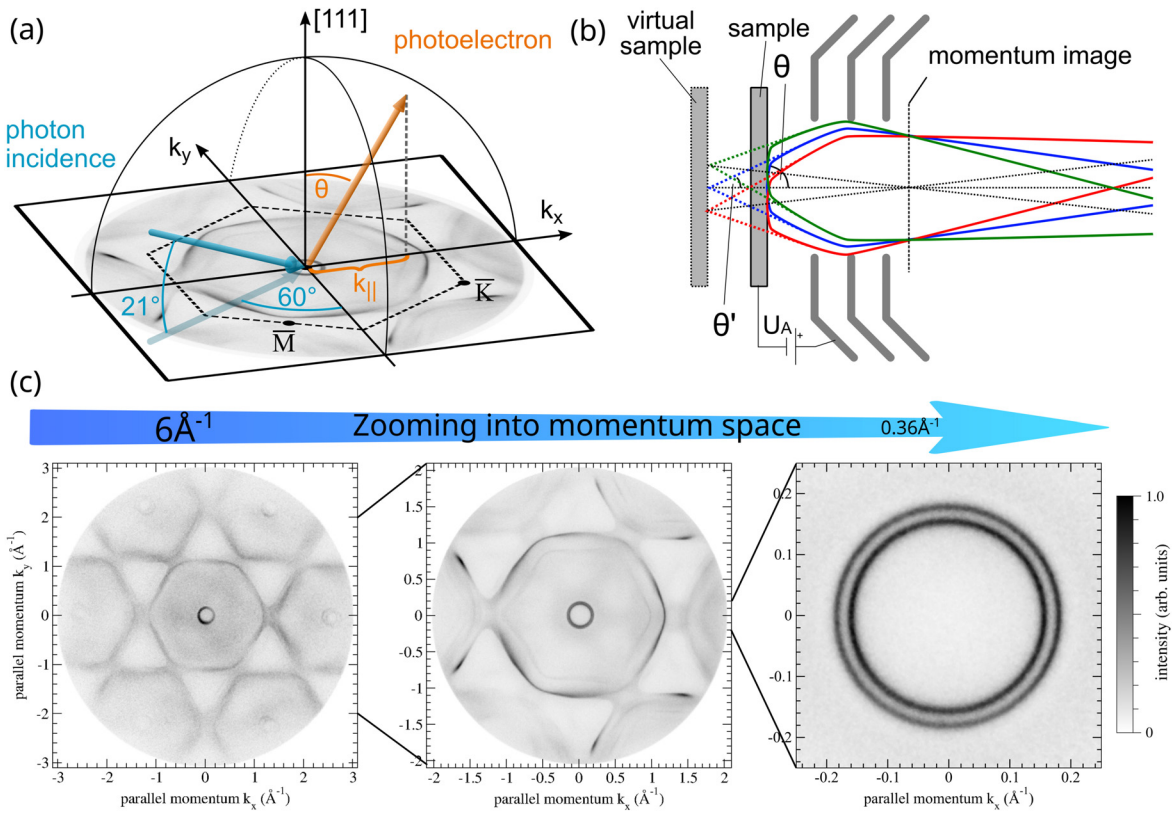

FIG. 2. (a) Geometry of a momentum microscope experiment. All photoelectrons emitted into the half-space above the sample surface are captured, and imaged as a 2D intensity distribution in the momentum image. Dashed lines indicate the fcc surface Brillouin zone. (b) Electrostatic immersion objective lens. The microscope sees a virtual sample with an effective finite emission angle θ'.[13] (c) Momentum space images with adjustable zoom in k-space. (b) Reprinted with permission from Suga and Tusche, J. Electron Spectrosc. Relat. Phenom. **200**, 119–142 (2015). Copyright 2015 Elsevier.

complex spin textures. Comprehensive maps of the spectral function $I\sigma(E_B, k_x, k_y, k_z)$ have already been measured for the prototypical ferromagnets iron[37] and cobalt,[8] revealing spin-dependent electron correlations and nonlocal effects in the ground-state electronic structure. Recently, emergent topological phases in a two-dimensional magnet have been discovered.[24] Figures 3(d)–3(f) demonstrate a significant change of the Fermi surface topology in the spin-resolved momentum maps of W(110), Fe(110), and the 2D hybrid ferromagnet consisting of 2MLs Fe on a W(110). For W(110) [Fig. 3(d)], the spin momentum adheres to time-reversal (TR) and mirror symmetries, while for the ferromagnet Fe(110) [Fig. 3(f)] the remanent magnetization M_y breaks TR symmetry. Note that the photon beam lies in the $y-z$ plane at an angle of 25° with respect to the sample surface. The observed intensity asymmetry between the upper and lower parts of the image, particularly in Fig. 3(f), arises from linear dichroism in the angular distribution (LDAD) due to the off-normal incidence of the light. This LDAD also has an immediate consequence for the measured spin polarization.[9,17,38]

Remarkably, the detailed spin-resolved momentum maps reveal a substantial change in the Fermi surface topology in the case of the ultrathin hybrid magnet Fe/W(110): the interplay of broken TR symmetry and strong spin–orbit coupling (SOC) leads to the formation of an interface-driven topological quantum phase, characterized by the emergence of highly spin-polarized giant open Fermi arcs at the left/right side of the SBZ in Fig. 3(e). Fermi arcs are the hallmark of monopole-like topological charges, so-called Weyl points (WP), inside a quantum material. Their ends are connected to sources and sinks of Berry flux in momentum space. The non-trivial band topology does not only affect transport but also the charge and spin dynamics in the material.[39]

3. Topological materials

The topologically non-trivial property of Dirac surface states, which are formed at the interface between a three-dimensional topological insulator (TI) and the vacuum, often manifests in "spin-momentum locked" spin textures.[40] Studies of the formation and spin texture of topological surface states (TSS) became a major use case of spin-resolving momentum microscopy, which today combines the demanding resolution requirements with spin resolution at every point in the momentum map. Figures 4(a) and 4(b) show the spin-resolved spectral function of the prototypical TI Bi_2Se_3. The Fermi surface contour, as well as the band dispersion along $\bar{M}-\bar{\Gamma}-\bar{M}$, were extracted from a large 3D dataset that consists of 40 constant-energy

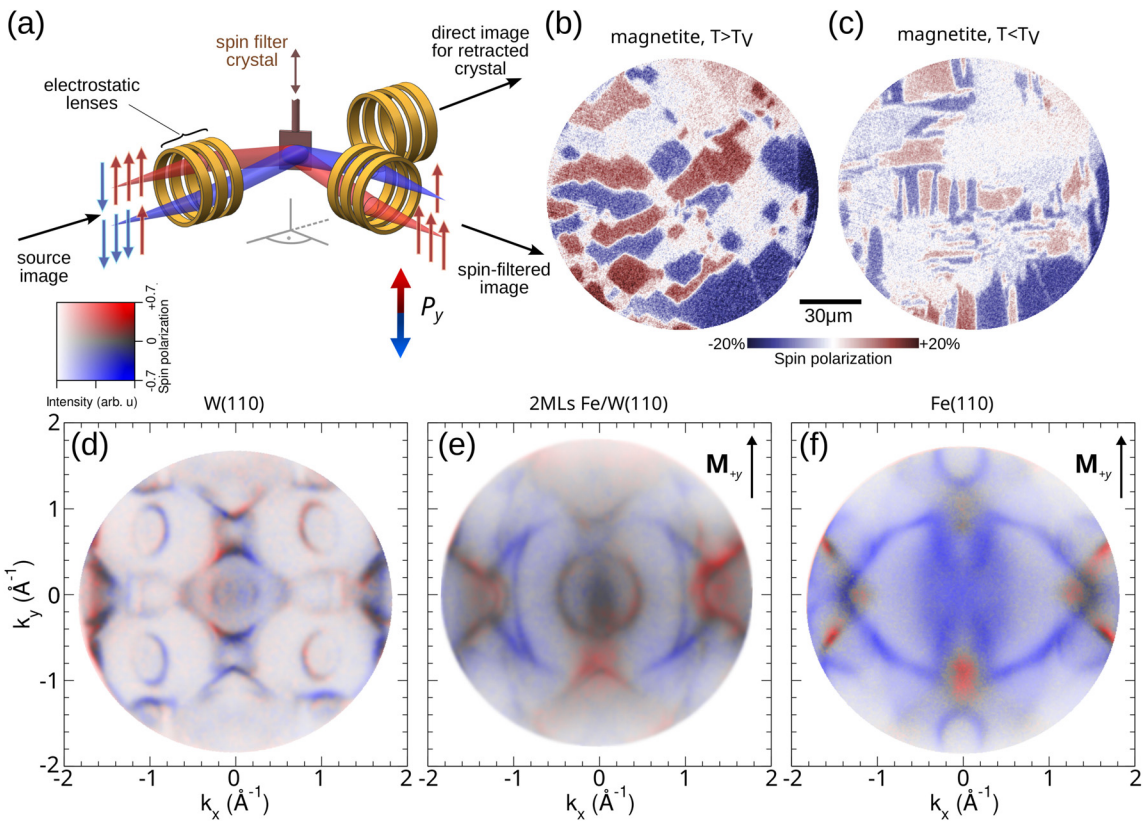

FIG. 3. Complex spin textures in real and momentum space. (a) Working principle of imaging spin filters.[1,27–29] (b) Spin-resolved PEEM measurements of a magnetite (Fe_3O_4) at 114 K (b) and 100 K (c).[7] (d)–(f) Significant change in the spin polarization in the Fermi surface of W(110),[32] Fe(110),[24] and the 2D hybrid ferromagnet Fe/W(110).[24] (e) and (f) The sample magnetization is oriented along the $+y$ direction. Measured intensities and spin polarizations are encoded using a 2D color code, where red and blue indicate the spin polarization P_y and the color saturation reflects the intensity. (b) and (c) Reprinted with permission from de la Figuera and Tusche, Appl. Surf. Sci. **391**, 66 (2016). Copyright 2016 Elsevier.

momentum images. Measured using HeI radiation ($h\upsilon = 21.2$ eV), the data comprise the full first SBZ and the neighboring SBZs, where the Dirac surface states appear with a clear spin polarization.

The TSS exhibits the characteristic spin-momentum-locking with spin-up states at positive k_x (red) and spin-down states at negative (blue) k_x around $\bar{\Gamma}$ at the Fermi energy E_F, as shown in Figs. 4(a) and 4(b).[9] The spin-momentum-locking is also present in the neighboring SBZs with varying spectral weights of the surface and bulk states. While the bulk conduction band (BCB) states near E_F exhibit no pronounced spin polarization, the measurement reveals strongly polarized states emerging from the bulk valence band starting at binding energies below E_F-1 eV. These results highlight the abundance of spin-polarized states in the near-surface electronic structure of Bi_2Se_3—a feature largely overlooked in most available spin-resolved photoemission studies, which typically focus on the TSS near the Fermi energy.

4. Van der Waals heterostructures

Two-dimensional (2D) materials, particularly sheets of transition metal dichalcogenides (TMDCs), can be stacked to form van der Waals heterostructures, allowing unprecedented flexibility for band structure engineering.[15,22,23] The design versatility is key to enabling future applications in electronics, optoelectronics and energy conversion.[41,42] It has been generally assumed that monosheets of TMDC's are bulk-like. In a single H-$TaSe_2$ monosheet, formed on a Bi_2Se_3(0001) surface, the central tantalum atom in the prismatic selenium environment, however, is vertically shifted.[22]

Lifting of the horizontal mirror symmetry in the sheet has important consequences: Figs. 4(c) and 4(d) show that the Fermi surface acquires an in-plane spin component. Despite the rather weak hybridization with the substrate, the chiral spin texture of the $TaSe_2$ monosheet is coupled to the helical spin texture of Bi_2Se_3.[22] Both spin textures appear as a superposition in the momentum maps in Figs. 4(c) and 4(d). Beyond topological and 2D van der Waals materials, spin-resolved momentum microscopy is widely applicable to a wide range of crystals with strong SOC.[1,2,19,20,32,43–47]

C. Mapping orbital states

Following theoretical proposals,[48] both linear and circular dichroism (CD) have been effectively employed to probe components of the orbital angular momentum (OAM) $L(\mathbf{k})$ of the electron wave function ψ_k.[49] The intrinsically fixed photoemission geometry of momentum microscopy measurements facilitates the application of quantitative

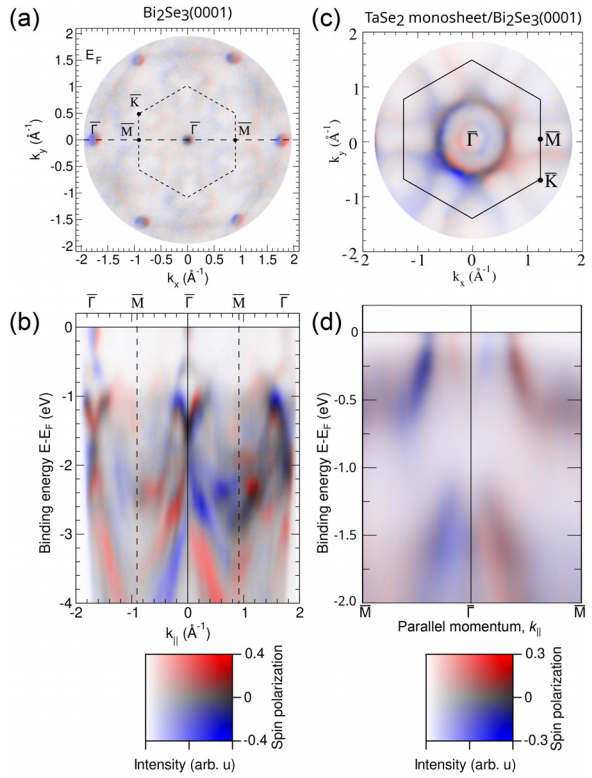

FIG. 4. (a) and (b) Spin-resolved Fermi surface of Bi_2Se_3 (a) and spectral function (b) along $\bar{M} - \bar{\Gamma} - \bar{M}$. (c) and (d) Spin-resolved 2D momentum map at the Fermi level (c) and band dispersions (d) of a H-$TaSe_2$ monosheet on Bi_2Se_3.[22] Measured intensities and spin polarizations are encoded using a 2D color code, where red and blue indicate the spin polarization P_y and the color saturation reflects the intensity. (c) and (d) Adapted with permission from Polyakov *et al.*, Nat. Commun. **13**, 2472 (2022). Copyright 2022 Author(s), licensed under a Creative Commons Attribution (CC BY) license.

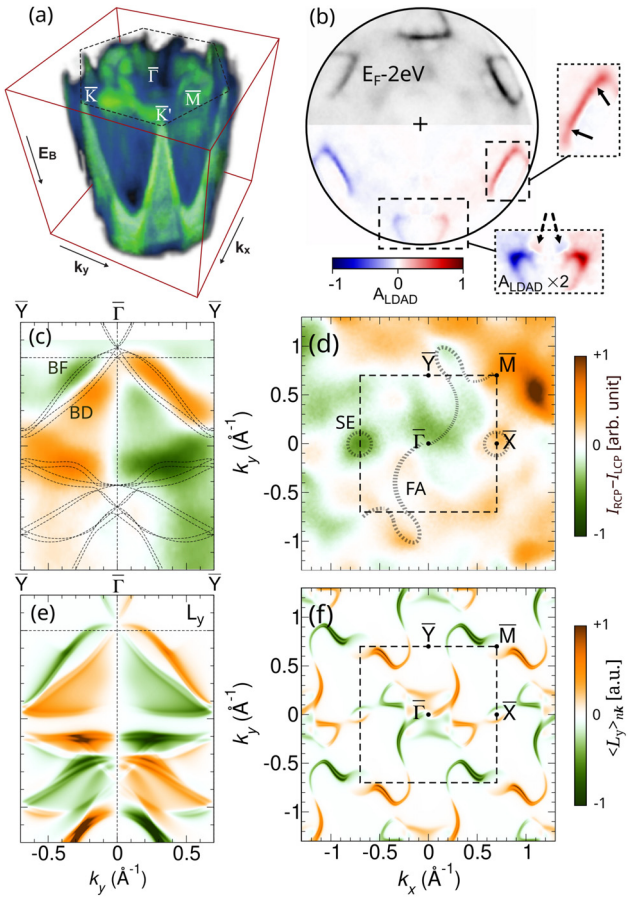

FIG. 5. Dichroism in momentum space. (a) Graphene on Ir(111) measured at $h\upsilon = 22$ eV.[18] The full 3D data matrix consists of 482 momentum disks shown in (b) on a linear gray scale (upper half) and LDAD (lower half). Arrows mark hybridization regions between the graphene π band and Ir-*d* states. (c) and (d) Measured an (e) and (f) theoretical OAM fingerprints of multifold chiral fermions ($h\upsilon = 56$ eV) in the bulk (c) and (e) and the helicoid Fermi ($h\upsilon = 78$ eV) arc (d) and (f) of the chiral topological semimetal CoSi.[12] (a) and (b) Reproduced with permission from Tusche *et al.*, Appl. Phys. Lett. **108**, 261602 (2016). Copyright 2016 AIP Publishing. (c)–(f) Reproduced with permission from Hagiwara *et al.*, Adv. Mater. **37**, 2418040 (2025). Copyright 2025 Author(s), licensed under a Creative Commons Attribution (CC BY) license.

models and the analysis of symmetry effects. In the simplest case, this additional information can be readily used to track the wave function contributions from different orbitals. For instance, *d*- and π-states of graphene on Ir(111) contribute with the LDAD of opposite sign, as shown in Fig. 5(b).[18] The LDAD is extracted from the 3D data matrix in Fig. 5(a). The 3D topology of the graphene π-band is observed with the six tips of the Dirac cones at the K points of the surface Brillouin zone.

The examination of CD in the angular distribution (CDAD) provides an even more comprehensive exploration of the Bloch wave function, including orbitals,[50,51] Berry curvature,[51,52] and topological invariants.[12] The OAM contribution to the CDAD can be intuitively understood by considering both the helicity of light and the self-rotation of the Bloch states.[48,50] In nonmagnetic materials, the combination of time-reversal and spatial inversion symmetries is a strong condition for orbital quenching, and dictates that OAM is absent for all states.[53] As a class of materials where an unquenched OAM is the main driver for their unusual physical proprieties, chiral crystals have recently attracted attention.

As a representative example, Fig. 5(c) shows the measured CD along a section through the multifold chiral fermion of the prototypical chiral semimetal CoSi. The observed CD represents the OAM L_y, which appears as an odd function of k_y in reminiscence of a monopole-like radial OAM texture $(\mathbf{K} \cdot \mathbf{L})$.[12] This gets quantitatively confirmed by the calculated L_y spectrum in Fig. 5(e). The CD and OAM maps in Figs. 5(d) and 5(f) reveal that the helicoid Fermi arcs inherit a pronounced OAM polarization from the chiral Fermions in the bulk.[12]

Results such as these provide important foundations for the concepts of "orbitronics," which aims to exploit the orbital degree of freedom as an information carrier in next-generation electronic devices.[53] Orbital-momentum locking makes topological chiral crystals an intriguing material platform for these recent developments. Momentum microscopy ultimately provides the orbital and phase

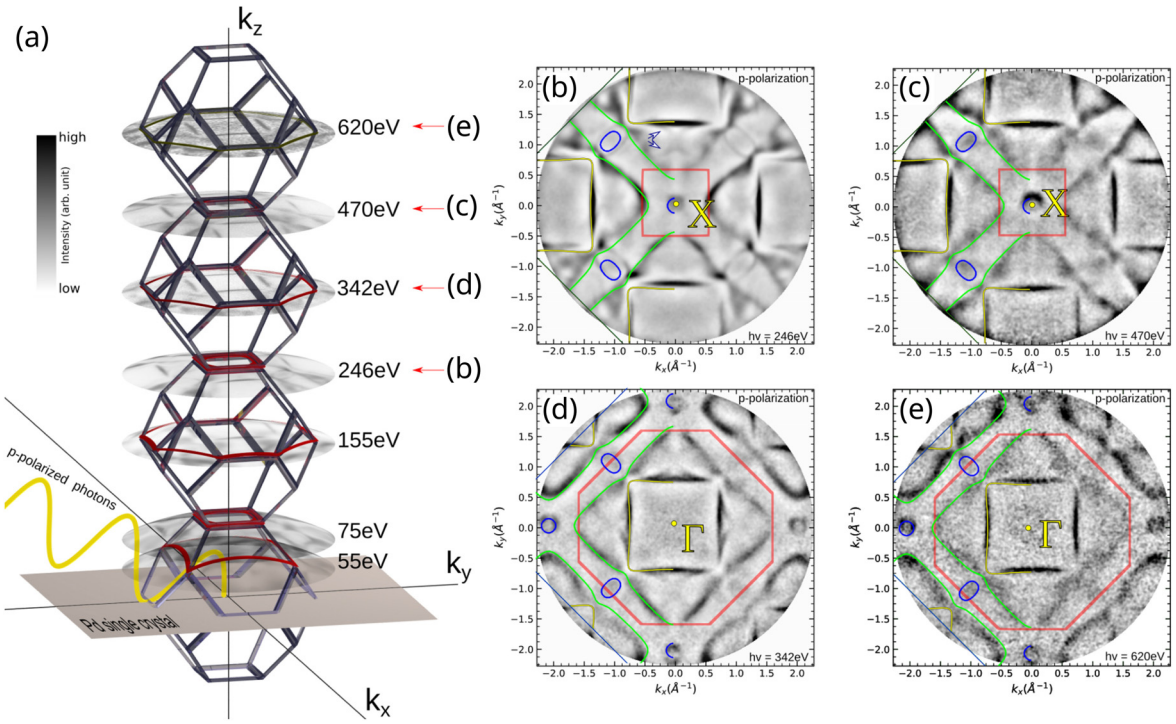

FIG. 6. Soft x-ray Fermi surface tomography of palladium. (a) Experimental geometry and isoenergy spherical cuts of the free electron final state in 3D momentum space, corresponding to the experimental momentum maps at the Fermi energy, obtained at soft x-ray photon energies of (b) 246 eV, (c) 470 eV, (d) 342 eV, and (e) 620 eV, respectively.[54] Reprinted with permission from Tan *et al.*, Ultramicroscopy **253**, 113820 (2023). Copyright 2023 Elsevier.

sensitivity required to access the full spin-orbital texture and to unveil the microscopic mechanisms of quantum transport phenomena like the orbital Hall effect and the orbital Edelstein effect.

D. (Spin-resolved) Fermi surface tomography

The Fermi surface describes the distribution of electrons at the boundary between occupied and unoccupied states. The shape and topology of the Fermi surface thus play a distinguished role in macroscopic properties, such as electric transport, heat capacity, and magnetism. Developing functional materials with specific physical properties involves engineering their Fermi surfaces. Well-known examples include high-temperature superconductors,[55] topological materials,[14,22,23,46] and half-metallic ferromagnets[56] for spintronic applications.

Momentum microscopy is a powerful tool for tomographically mapping the electron states in the entire 3D Fermi surface.[8,54,57] Figures 6(a)–6(e) show soft x-ray Fermi surface tomography of palladium.[54] Figures 6(b) and 6(c) show sections through the *X*-point of the BZ, while Figs. 6(d) and 6(e) feature those cutting through the BZ center. Notably, there is a remarkable overall consistency in the Fermi surface topology between the third ($h\upsilon = 246$ eV, $h\upsilon = 342$ eV) and fourth zones ($h\upsilon = 470$ eV, $h\upsilon = 620$ eV). This approach facilitates the reconstruction of detailed three-dimensional spectral responses in momentum space.[54]

The concept of Fermi surface tomography can also be extended to ferromagnets, where the Fermi surface consists of sheets for majority (↑) and minority (↓) electrons. The spin-resolved Fermi surface of ferromagnetic cobalt has been measured in the full BZ by spin-resolving momentum microscopy. The results showed that nonlocal effects are decisive for the spin-dependent interactions in cobalt and other ferromagnets.[8] Such nonlocal electron correlations are still difficult to model. Advanced theories are just emerging and need

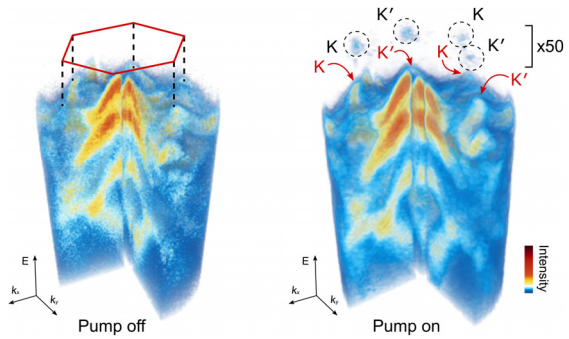

FIG. 7. Momentum microscopy of non-equilibrium electronic states of the 2D semiconductor WSe_2 after optical excitation with intense 775 nm light pulses.[10] WSe_2 exhibits a hexagonal Brillouin zone. Excited states above the Fermi energy are observed around the K and K′ symmetry points, and subsequently decay into the energetically lower Σ and Σ′ valleys.[10] Reproduced with permission from Kutnyakhov *et al.*, Rev. Sci. Instrum. **91**, 013109 (2020). Copyright 2020 AIP Publishing.

quantitative experimental input.[37] The findings that become possible by use of spin-resolving momentum microscopy thus substantially affect our understanding of electron interactions in solids.

E. Ultrafast quantum dynamics

Going beyond static imaging and being able to address dynamic processes is one of the current grand challenges in electron spectroscopy and microscopy. The efficient parallel imaging approach of an electron microscope is particularly useful when adding the additional dimension of time to the experiment. As an example, Fig. 7 shows the electron dynamics of the 2D semiconductor WSe_2, which has been measured at the free electron laser (FEL) FLASH (Hamburg).[10] This pioneering experiment demonstrates the feasibility of time-resolved photoelectron spectroscopy experiments by use of a parallel imaging momentum microscope.

Despite the low pulse repetition rate of the free electron laser (FEL), an advanced time-of-flight energy analyzer[4,15,18] allows for the simultaneous acquisition of the complete 3D spectral function, $I(k_x, k_y, E_B)$, within a few hours. The results reveal the correlated dynamics at different momentum points: in particular, excitation by 775 nm infrared pulses populates non-equilibrium states at the K and K′ valleys. The comprehensive data reveal that subsequent decay dynamics mainly take place via inter-valley scattering into the energetically lower Σ and Σ′ valleys.[10] Due to spin-valley locking in individual layers,[58,59] the observed population dynamics has immediate consequences for ultrafast spin excitations and the optical control of spin currents.

F. Buried interfaces and operando characterization of electronic devices

The functional region of most electronic devices is not easily accessible. The function often relies on processes at internal interfaces, such as the conduction channel formation below the gate electrode of a MOS-FET, the redox reactions at the electrode–electrolyte interfaces of a battery, or the oxygen vacancy movement in oxide based resistive switches. Additionally, the region of interest is buried under further material layers that serve as insulation, tunnel barrier, or contact electrodes. Other layers are inevitably formed during sample processing, such as native oxide layers and contamination, and cannot be removed without modifying the functional layer.

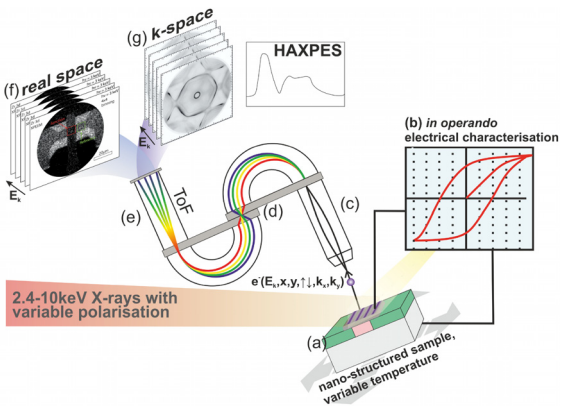

FIG. 8. Operando characterization of functional devices. The figure shows (a) an electrically contacted sample with (b) electric and (c) spectroscopic characterization. Photoelectrons from the sample (a) are collected by the hybrid momentum microscope (c), pre-filtered by hemispherical analyzers (d), and analyzed with high energy resolution in ToF drift section (e). Colors illustrate different electron energies. Images are recorded with (f) spatial and (g) momentum resolution.

In order to access the functional region several nanometers beneath the surface, one thus needs to work at significantly higher energies where the electrons' mean free path is long enough.[60] Hard x-ray photoemission spectroscopy (HAXPES) has been shown to reach an information depth of up to 57 nm at an electron kinetic energy of 15 keV.[61] HAXPES has already been effectively combined with PEEM,[62,63] and has been applied to investigate resistive switching devices,[64] and recent studies used HX-excitation in PEEM to investigate corrosion mechanisms on steels.[65] Presently an information depth of 5 nm at a spatial resolution of 1 μm marks the limits of current instrumentation. The reason lies in the detrimental effects of reduced photoionization cross sections and low instrumental transmission at high electron kinetic energies, which also points out directions for improvement: While cross sections are defined by physics, instrument transmission and signal detection can be optimized by instrument design. In particular, a combination of HAXPES with momentum microscopy is a promising experimental approach that will give access to electronic states at buried interfaces or in the bulk.

The term *in operando* refers to experiments performed not on model systems, but on working electronic devices like transistors, capacitors, batteries, and switches during operation, to gain insight into the processes and phenomena that constitute their functionality or cause their failure. This information is naturally of high interest for device optimization and failure analysis.

An important technical part of in operando experiments is the wiring of the electronic devices under investigation in a PEEM environment, which includes high electric fields, high voltage sample biasing, and UHV conditions. On the contrary, the nano-structured devices need carefully controlled low operating voltages under current compliance. Since HV discharges between the objective lens and the sample cannot be excluded in PEEM, surge protection for the device circuitry is mandatory. Some promising solutions to these technical issues have already been published.[66,67] Especially the use of UHV compatible printed circuit board chips on sample holders as described in Ref. 67 could facilitate mounting samples that need a lot of contacts established by wire bonding.

IV. CONCLUSION AND FUTURE PERSPECTIVES

Momentum microscopy provides imaging of micro- and nanostructures in real-space, momentum-resolved maps of the electronic states in reciprocal space and across the entire 3D Brillouin zone, as well as spin-resolved maps of complex spin textures. With the recent addition of time resolution, covering the typical time scales of the electron and spin subsystems, an "All-in-One" experiment, as outlined in Fig. 1, is now within reach. Notably, momentum microscopy has been applied to a broad range of materials, including metals and ferromagnets, organic thin films, bulk and thin-film oxides, and topological quantum materials. The discovery of topological protection in condensed matter systems, with corresponding unusual spin-properties of the underlying electron wave functions, has created a huge demand for spin-resolved electron spectroscopy experiments.

Hard x-ray excitation enables spectroscopic access to electronic and chemical information from deep within materials, for example, probing through overlayers or electrodes of devices. A promising future direction is to combine two complementary approaches: dispersive analyzers based on a configuration of two hemispheres with time-of-flight based electron recording, as outlined in Fig. 8. By combining the imaging and spectroscopic capabilities of momentum microscopy, such an instrument will drive technological and scientific advances in fields as diverse as battery, corrosion, and materials science, as well as electrical engineering and quantum technology.

While synchrotron- or FEL-based experiments remain highly challenging, laboratory scale laser sources in the XUV (extreme ultraviolet) to soft x-ray energy range are becoming available, based on the principle of high harmonic generation in noble gases.[15,68] With laser repetition rates that reach up to 10 MHz, such sources can make ideal use of the highest efficiency of momentum microscopy, reducing the acquisition times by several orders of magnitude.[69] This advancement opens the way for incorporating electron- and spin dynamics into time-resolved momentum microscopy experiments.

ACKNOWLEDGMENTS

The authors like to acknowledge J. Kirschner (MPI-Halle), G. Schönhense (Uni-Mainz), and S. Suga (Uni-Osaka) for a long and fruitful collaboration, enduring interest, and inspiration in the development of momentum microscopy and imaging electron spin filters. The authors further like to thank H. L. Meyerheim (MPI-Halle), J. Henk (Uni-Halle), A. Ernst (Uni-Linz), H.-J. Elmers, D. Go (Uni-Mainz), M.-T. Lin, G.-J. Shu (Nat. Taipei Univ.), Y. Mokrousov, S. Blügel, G. Bihlmayer, V. Feyer, X. L. Tan, K. Hagiwara, and R. Dunin-Borkowski (FZ-Jülich) for fruitful cooperation and numerous joint experiments. Funding by the Federal Ministry of Education and Research (BMBF, Grant Nos. 05K16PGB and 05K19PGA) and by the Federal Ministry of Research, Technology and Space (BMFTR, Grant No. 05K25PGB) is gratefully acknowledged.

AUTHOR DECLARATIONS

Conflict of Interest

The authors have no conflicts to disclose.

Author Contributions

Ying-Jiun Chen: Conceptualization (equal); Data curation (lead); Formal analysis (lead); Investigation (equal); Supervision (equal); Visualization (lead); Writing – original draft (lead); Writing – review & editing (equal). **Carsten Wiemann:** Data curation (equal); Formal analysis (equal); Investigation (equal); Visualization (supporting); Writing – original draft (supporting); Writing – review & editing (equal). **Wei-Sheng Chiu:** Data curation (supporting); Formal analysis (equal); Investigation (equal); Visualization (equal); Writing – review & editing (equal). **Christoph Schlueter:** Formal analysis (supporting); Investigation (equal); Visualization (equal); Writing – original draft (supporting); Writing – review & editing (equal). **Claus M. Schneider:** Conceptualization (equal); Funding acquisition (equal); Resources (equal); Writing – review & editing (equal). **Christian Tusche:** Conceptualization (lead); Data curation (equal); Formal analysis (equal); Funding acquisition (equal); Investigation (lead); Project administration (lead); Resources (equal); Supervision (lead); Writing – original draft (equal); Writing – review & editing (equal).

DATA AVAILABILITY

The data that support the findings of this study are available from the corresponding author upon reasonable request.

REFERENCES

[1]C. Tusche, A. Krasyuk, and J. Kirschner, Ultramicroscopy **159**, 520 (2015).
[2]C. Tusche, Y.-J. Chen, L. Plucinski, and C. M. Schneider, e-J. Surf. Sci. Nanotechnol. **18**, 48 (2020).
[3]C. Tusche, K. Hagiwara, X. Tan, Y.-J. Chen, and C. Schneider, J. Vac. Sci. Technol. B **41**, 042201 (2023).
[4]C. Tusche, A. Krasyuk, J. Kirschner, and G. Schönhense, "Messvorrichtung und Verfahren zur Erfassung einer Impulsverteilung geladener Teilchen," German patent DE102013005173C5 (2014).
[5]D. Hartung, J. Kirschner, and C. Tusche, "Elektrodenträgereinrichtung und elektronen-optische Linse für elektrisch geladene Teilchen sowie deren Verwendung," German patent DE102014018555B3 (2016).
[6]C. Tusche and J. Kirschner, "Abbildende Energiefiltervorrichtung und Verfahren zu deren Betrieb," German patent DE102014019408B4 (2016).
[7]J. de la Figuera and C. Tusche, Appl. Surf. Sci. **391**, 66 (2016).
[8]C. Tusche, M. Ellguth, V. Feyer, A. Krasyuk, C. Wiemann, J. Henk, C. M. Schneider, and J. Kirschner, Nat. Commun. **9**, 3727 (2018).
[9]H. L. Meyerheim and C. Tusche, Phys. Status Solidi RRL **12**, 1800078 (2018).
[10]D. Kutnyakhov, R. P. Xian, M. Dendzik, M. Heber, F. Pressacco, S. Y. Agustsson, L. Wenthaus, H. Meyer, S. Gieschen, G. Mercurio *et al.*, Rev. Sci. Instrum. **91**, 013109 (2020).
[11]D. Curcio, S. Pakdel, K. Volckaert, J. A. Miwa, S. Ulstrup, N. Lanatà, M. Bianchi, D. Kutnyakhov, F. Pressacco, G. Brenner *et al.*, Phys. Rev. B **104**, L161104 (2021).
[12]K. Hagiwara, Y. Chen, D. Go, X. L. Tan, S. Grytsiuk, K. O. Yang, G. Shu, J. Chien, Y. Shen, X. Huang *et al.*, Adv. Mater. **37**, 2418040 (2025).
[13]S. Suga and C. Tusche, J. Electron Spectrosc. Relat. Phenom. **200**, 119–142 (2015).
[14]A. Cavallin, V. Sevriuk, K. N. Fischer, S. Manna, S. Ouazi, M. Ellguth, C. Tusche, H. L. Meyerheim, D. Sander, and J. Kirschner, Surf. Sci. **646**, 72–82 (2015).
[15]M. Aeschlimann, J. P. Bange, M. Bauer, U. Bovensiepen, H.-J. Elmers, T. Fauster, L. Gierster, U. Höfer, R. Huber, A. Li *et al.*, Surf. Sci. **753**, 122631 (2025).
[16]C. Tusche, Y.-J. Chen, C. M. Schneider, and J. Kirschner, Ultramicroscopy **206**, 112815 (2019).
[17]S. Suga, A. Sekiyama, and C. Tusche, *Photoelectron Spectroscopy: Bulk and Surface Electronic Structures*, 2nd ed. (Springer International Publishing, 2021), Chap. 11, pp. 351–416.
[18]C. Tusche, P. Goslawski, D. Kutnyakhov, M. Ellguth, K. Medjanik, H. J. Elmers, S. Chernov, R. Wallauer, D. Engel, A. Jankowiak *et al.*, Appl. Phys. Lett. **108**, 261602 (2016).
[19]D. Kutnyakhov, S. Chernov, K. Medjanik, R. Wallauer, C. Tusche, M. Ellguth, S. A. Nepijko, M. Krivenkov, J. Braun, S. Borek *et al.*, Sci. Rep. **6**, 29394 (2016).
[20]H. J. Elmers, R. Wallauer, M. Liebmann, J. Kellner, M. Morgenstern, R. N. Wang, J. E. Boschker, R. Calarco, J. Sánchez-Barriga, O. Rader *et al.*, Phys. Rev. B **94**, 201403(R) (2016).
[21]O. Karni, I. Esin, and K. M. Dani, Adv. Mater. **35**, e2204120 (2023).
[22]A. Polyakov, K. Mohseni, R. Felici, C. Tusche, Y.-J. Chen, V. Feyer, J. Geck, T. Ritschel, A. Ernst, J. Rubio-Zuazo *et al.*, Nat. Commun. **13**, 2472 (2022).
[23]A. Polyakov, K. Mohseni, G. R. Castro, J. Rubio-Zuazo, A. Zeugner, A. Isaeva, Y.-J. Chen, C. Tusche, and H. L. Meyerheim, Sci. Rep. **9**, 4052 (2019).
[24]Y.-J. Chen, J.-P. Hanke, M. Hoffmann, G. Bihlmayer, Y. Mokrousov, S. Blügel, C. M. Schneider, and C. Tusche, Nat. Commun. **13**, 5309 (2022).
[25]J. Henk, M. Hoesch, J. Osterwalder, A. Ernst, and P. Bruno, J. Phys.: Condens. Matter **16**, 7581 (2004).

[26]J. Henk, A. Ernst, and P. Bruno, Phys. Rev. B **68**, 165416 (2003).
[27]C. Tusche, M. Ellguth, A. A. Ünal, C.-T. Chiang, A. Winkelmann, A. Krasyuk, M. Hahn, G. Schönhense, and J. Kirschner, Appl. Phys. Lett. **99**, 032505 (2011).
[28]C. Tusche, M. Ellguth, A. Krasyuk, A. Winkelmann, D. Kutnyakhov, P. Lushchyk, K. Medjanik, G. Schönhense, and J. Kirschner, Ultramicroscopy **130**, 70 (2013).
[29]D. Vasilyev, C. Tusche, F. Giebels, H. Gollisch, R. Feder, and J. Kirschner, J. Electron Spectrosc. Relat. Phenom. **199**, 10 (2015).
[30]D. Kutnyakhov, P. Lushchyk, A. Fognini, D. Perriard, M. Kolbe, K. Medjanik, E. Fedchenko, S. Nepijko, H. Elmers, G. Salvatella *et al.*, Ultramicroscopy **130**, 63 (2013).
[31]T. J. Gay and F. B. Dunning, Rev. Sci. Instrum. **63**, 1635 (1992).
[32]Y.-J. Chen, M. Hoffmann, B. Zimmermann, G. Bihlmayer, S. Blügel, C. M. Schneider, and C. Tusche, Commun. Phys. **4**, 179 (2021).
[33]E. J. W. Verwey, Nature **144**, 327 (1939).
[34]K. Abe, Y. Miyamoto, and S. Chikazumi, J. Phys. Soc. Jpn. **41**, 1894 (1976).
[35]C. Ziethen, O. Schmidt, G. H. Fecher, C. M. Schneider, G. Schönhense, R. Frömter, M. Seider, K. Grzelakowski, M. Merkel, D. Funnemann *et al.*, J. Electron Spectrosc. Relat. Phenom. **88–91**, 983 (1998).
[36]M. Cinchetti, A. Gloskovskii, S. A. Nepjiko, G. Schönhense, H. Rochholz, and M. Kreiter, Phys. Rev. Lett. **95**, 047601 (2005).
[37]E. Młyńczak, M. C. T. D. Müller, P. Gospodarič, T. Heider, I. Aguilera, G. Bihlmayer, M. Gehlmann, M. Jugovac, G. Zamborlini, C. Tusche *et al.*, Nat. Commun. **10**, 505 (2019).
[38]N. A. Cherepkov and G. Schönhense, Europhys. Lett. **24**, 79 (1993).
[39]Y.-J. Chen, T.-H. Chuang, J.-P. Hanke, Y. Mokrousov, S. Blügel, C. M. Schneider, and C. Tusche, Appl. Phys. Lett. **124**, 093105 (2024).
[40]M. Z. Hasan and C. L. Kane, Rev. Mod. Phys. **82**, 3045 (2010).
[41]J. F. Sierra, J. Fabian, R. K. Kawakami, S. Roche, and S. O. Valenzuela, Nat. Nanotechnol. **16**, 856 (2021).
[42]K. S. Novoselov, A. Mishchenko, A. Carvalho, and A. H. Castro Neto, Science **353**, aac9439 (2016).
[43]P. M. Sheverdyaeva, G. Bihlmayer, S. Modesti, V. Feyer, M. Jugovac, G. Zamborlini, C. Tusche, Y.-J. Chen, X. L. Tan, K. Hagiwara *et al.*, Nanoscale **16**, 15815 (2024).
[44]H. Bentmann, H. Maaß, J. Braun, C. Seibel, K. A. Kokh, O. E. Tereshchenko, S. Schreyeck, K. Brunner, L. W. Molenkamp, K. Miyamoto *et al.*, Phys. Rev. B **103**, L161107 (2021).
[45]P. M. Sheverdyaeva, D. Pacilè, D. Topwal, U. Manju, M. Papagno, V. Feyer, M. Jugovac, G. Zamborlini, I. Cojocariu, C. Tusche *et al.*, Phys. Rev. B **106**, 045108 (2022).
[46]A. Polyakov, C. Tusche, M. Ellguth, E. D. Crozier, K. Mohseni, M. M. Otrokov, X. Zubizarreta, M. G. Vergniory, M. Geilhufe, E. V. Chulkov *et al.*, Phys. Rev. B **95**, 180202(R) (2017).
[47]H. Maaß, H. Bentmann, C. Seibel, C. Tusche, S. V. Eremeev, T. R. F. Peixoto, O. E. Tereshchenko, K. A. Kokh, E. V. Chulkov, J. Kirschner *et al.*, Nat. Commun. **7**, 11621 (2016).
[48]J.-H. Park, C. H. Kim, J.-W. Rhim, and J. H. Han, Phys. Rev. B **85**, 195401 (2012).
[49]M. Ünzelmann, H. Bentmann, P. Eck, T. Kißlinger, B. Geldiyev, J. Rieger, S. Moser, R. C. Vidal, K. Kißner, L. Hammer *et al.*, Phys. Rev. Lett. **124**, 176401 (2020).
[50]S. S. Brinkman, X. L. Tan, B. Brekke, A. C. Mathisen, Ø. Finnseth, R. J. Schenk, K. Hagiwara, M.-J. Huang, J. Buck, M. Kalläne *et al.*, Phys. Rev. Lett. **132**, 196402 (2024).
[51]M. Ünzelmann, H. Bentmann, T. Figgemeier, P. Eck, J. N. Neu, B. Geldiyev, F. Diekmann, S. Rohlf, J. Buck, M. Hoesch *et al.*, Nat. Commun. **12**, 3650 (2021).
[52]Y. Liu, G. Bian, T. Miller, and T.-C. Chiang, Phys. Rev. Lett. **107**, 166803 (2011).
[53]D. Go, D. Jo, H.-W. Lee, M. Kläui, and Y. Mokrousov, Europhys. Lett. **135**, 37001 (2021).
[54]X. L. Tan, K. Hagiwara, Y.-J. Chen, J. Schusser, I. Cojocariu, D. Baranowski, V. Feyer, J. Minár, C. M. Schneider, and C. Tusche, Ultramicroscopy **253**, 113820 (2023).
[55]J. A. Sobota, Y. He, and Z.-X. Shen, Rev. Mod. Phys. **93**, 025006 (2021).
[56]X. L. Tan, A. Ernst, K. Hagiwara, Y.-J. Chen, C. M. Schneider, and C. Tusche, Phys. Rev. Lett. **135**, 036703 (2025).
[57]H. J. Elmers, D. Kutnyakhov, S. V. Chernov, K. Medjanik, O. Fedchenko, A. Zaporozhchenko-Zymakova, M. Ellguth, C. Tusche, J. Viefhaus, and G. Schönhense, J. Phys.: Condens. Matter **29**, 255001 (2017).
[58]R. Bertoni, C. Nicholson, L. Waldecker, H. Hübener, C. Monney, U. D. Giovannini, M. Puppin, M. Hoesch, E. Springate, R. Chapman *et al.*, Phys. Rev. Lett. **117**, 277201 (2016).
[59]G. Wang, A. Chernikov, M. M. Glazov, T. F. Heinz, X. Marie, T. Amand, and B. Urbaszek, Rev. Mod. Phys. **90**, 021001 (2018).
[60]C. J. Powell, J. Vac. Sci. Technol. A **38**, 023209 (2020).
[61]J. Rubio-Zuazo and G. Castro, Appl. Surf. Sci. **599**, 153918 (2022).
[62]C. Wiemann, M. Patt, S. Cramm, M. Escher, M. Merkel, A. Gloskovskii, S. Thiess, W. Drube, and C. M. Schneider, Appl. Phys. Lett. **100**, 223106 (2012).
[63]M. Patt, C. Wiemann, N. Weber, M. Escher, A. Gloskovskii, W. Drube, M. Merkel, and C. M. Schneider, Rev. Sci. Instrum. **85**, 113704 (2014).
[64]A. Kindsmüller, C. Schmitz, C. Wiemann, K. Skaja, D. J. Wouters, R. Waser, C. M. Schneider, and R. Dittmann, APL Mater. **6**, 046106 (2018).
[65]X. Yue, D. Chen, A. Krishnan, I. Lazar, Y. Niu, E. Golias, C. Wiemann, A. Gloskovskii, C. Schlueter, A. Jeromin *et al.*, J. Mater. Sci. Technol. **205**, 191 (2025).
[66]M. Buzzi, C. A. F. Vaz, J. Raabe, and F. Nolting, Rev. Sci. Instrum. **86**, 083702 (2015).
[67]M. Foerster, J. Prat, V. Massana, N. Gonzalez, A. Fontsere, B. Molas, O. Matilla, E. Pellegrin, and L. Aballe, Ultramicroscopy **171**, 63 (2016).
[68]S. Hädrich, J. Rothhardt, M. Krebs, S. Demmler, A. Klenke, A. Tünnermann, and J. Limpert, J. Phys. B **49**, 172002 (2016).
[69]M. Büscher, R. Adam, C. Tusche, A. Hützen, C. Wiemann, Y.-J. Chen, and C. M. Schneider, JLSRF **6**, A138 (2020).